Structure and dynamics of solvated polyethylenimine chains

Titus A. Beu, and Alexandra Farcaş

Citation: AIP Conference Proceedings **1916**, 020001 (2017);
View online: https://doi.org/10.1063/1.5017421
View Table of Contents: http://aip.scitation.org/toc/apc/1916/1
Published by the American Institute of Physics

Structure and Dynamics of Solvated Polyethylenimine Chains

Titus A. Beu[1,a)] and Alexandra Farcaş[1]

[1]*Department of Biomolecular Physics, Faculty of Physics, University Babeş-Bolyai, Mihail Kogălniceanu Street 1, Cluj-Napoca 400084, Romania*

[a)]Corresponding author: titus.beu@phys.ubbcluj.ro

Abstract. Polimeric gene-delivery carriers have attracted great interest in recent years, owing to their applicability in gene therapy. In particular, cationic polymers represent the most promising delivery vectors for nucleic acids into the cells. This study presents extensive atomistic molecular dynamics simulations of linear polyethylenimine chains. The simulations show that the variation of the chain size and protonation fraction causes a substantial change of the diffusion coefficient. Examination of the solvated chains suggests the possibility of controlling the polymer diffusion mobility in solution.

INTRODUCTION

Gene therapy is a therapeutic technique which involves the insertion of genomic material into cells for the treatment of various diseases [1, 2]. Different types of gene delivery systems for somatic cells by *viral* and *nonviral* systems are applied to restore specific gene functions [3]. The most efficient delivery agents are viral vectors, which are nevertheless limited by their potential toxicity [4]. On the other hand, nonviral systems, such as cationic polymers, offer the advantage of low production cost, reduced toxicity, accessible chemistry, validating them as a promising class of delivery vectors for gene therapy [5]. Among the synthetic polymers, polyethylenimine (PEI) features a combination of properties (charge, size, and stability), which favor adequate release and protection of the gene [6].

PEI is an organic polycation with a relatively high transfection efficiency as a gene delivery vector, and it has been employed in a large variety of drug delivery systems [7, 8]. Moreover, as compared to other polycations, PEI shows the ability to more effectively protect DNA from enzyme degradation. Depending on the spatial arrangement of the composing NH and CH_2 groups, PEI can be either linear or branched. The effectiveness of PEI as a gene delivery vector is attributed to its particular charge distribution. The positively charged amino groups of PEI enable strong interactions with the negatively charged phosphate groups of DNA and cause the condensation of the latter [8]. PEI-DNA polyplexes enter cells through endocytosis and, while the endosomal compartments increase their acidity, PEI may increase its protonation state and may act as a proton sponge, adsorbing some of the entering protons. The proton sponge effect is commonly used to explain the release mechanism of the polyplexes from endosomes [9, 10]. Furthermore, the change of the PEI protonation state inside the endosomes is also believed to cause the release of the DNA from the polyplexes [10].

Notwithstanding the acknowledged importance of the condensation and proton sponge effects, the structural dynamics of solvated PEI (including as part of DNA-PEI polyplexes) is only qualitatively understood, and the reported protonation-related behavior of PEI is rather inconsistent [11]. Numerical simulations, in particular, have not yet been able to provide significantly advanced insight in this respect. Among the representative simulations of solvated PEI and DNA/PEI complexes are those of Zierbarth et al. [11], Sun et al. [12], and Wei et al. [13].

METHODS

Molecular dynamics (MD) simulations of complex bio-molecular systems require realistic force fields to describe the interactions between the components. We used the well-established additive all-atom force field model

TIM17 Physics Conference
AIP Conf. Proc. 1916, 020001-1–020001-6; https://doi.org/10.1063/1.5017421
Published by AIP Publishing. 978-0-7354-1608-6/$30.00

CHARMM [14, 15], having the functional form:

$$U_{bonded} = \sum_{bonds} k_b (b - b_0)^2 + \sum_{angles} k_\theta (\theta - \theta_0)^2 + \sum_{dihedrals} k_\psi [1 + \cos(n\psi - \delta)] + \sum_{impropers} k_\omega (\omega - \omega_0)^2 + \sum_{Urey-Bradley} k_{UB} \left(b^{1,3} - b_0^{1,3}\right)^2, \quad (1)$$

$$U_{non-bonded} = \sum_{atomsi,j} \frac{q_i q_j}{\epsilon_0 r_{ij}} + \varepsilon_{ij} \left[\left(\frac{r_{ij}^{min}}{r_{ij}} \right)^{12} - 2 \left(\frac{r_{ij}^{min}}{r_{ij}} \right)^{6} \right], \quad (2)$$

$$r_{ij}^{min} = \left(r_i^{min} + r_j^{min}\right)/2, \quad \epsilon_{ij} = \sqrt{\epsilon_i \epsilon_j}. \quad (3)$$

Here, the bonded contributions (Equation (1)) are modeled by harmonic terms for bonds, angles, dihedrals, and improper angles, while the non-bonded interactions (Equation (2)) are represented by Coulomb and Lennard-Jones terms.

In our extensive MD simulations, we employed the highly scalable code NAMD [16]. Specifically, we used the built-in Velocity Verlet integrator to propagate the particle trajectories with a time step of 2 fs, and the SHAKE algorithm [17] to constrain the covalent bonds involving hydrogen atoms. A cutoff distance of 12 Å was applied to the van der Waals and real-space electrostatic interactions, with a switching function setting in at 10 ÅThe Particle Mesh Ewald (PME) [18] method was employed to treat long-range electrostatic interactions on a 3D grid with a spacing of 1 Å. The systems were simulated within the NPT ensemble, fixing the pressure at 1 atm and the temperature at 310 K using, respectively, a Langevin piston and a Langevin thermostat with a damping coefficient of 1 ps^{-1}. All the illustrations resulted from the simulations were generated using the VMD package [19].

RESULTS

To gain better understanding on how the size and degree of protonation affect the dynamics of solvated linear PEI chains, we employed the force field for unprotonated/protonated PEI that we recently developed [20]. Each simulated system consisted of a PEI chain composed of 14, 26, and 50-mers, with protonation fractions equal to 0, 1/2, 1/3, and 1/4.

The polymers were solvated in TIP3P water [21], with the size of the cubic simulation box ranging from 17 Å (14-mers) to 45 Å (50-mers). The water boxes were created sufficiently large to screen the interactions between the polymer chains and their periodic images. Monovalent counterions (Cl^-) were added to the system in order to neutralize the protonation charges of the polymer chains. The details of each simulated system are summarized in Table 1.

TABLE 1. Basic data defining the simulated systems.

Chain length	Protonation fraction	No. of PEI atoms	No. of Cl^- ions	Total no. of atoms
14-mers	0	116	0	4160
	1/4	119	3	4145
	1/3	120	4	4144
	1/2	122	6	4145
26-mers	0	212	0	20258
	1/4	218	6	20267
	1/3	220	8	20256
	1/2	224	12	20243
50-mers	0	404	0	69500
	1/4	416	12	69476
	1/3	420	16	69457
	1/2	428	24	69449

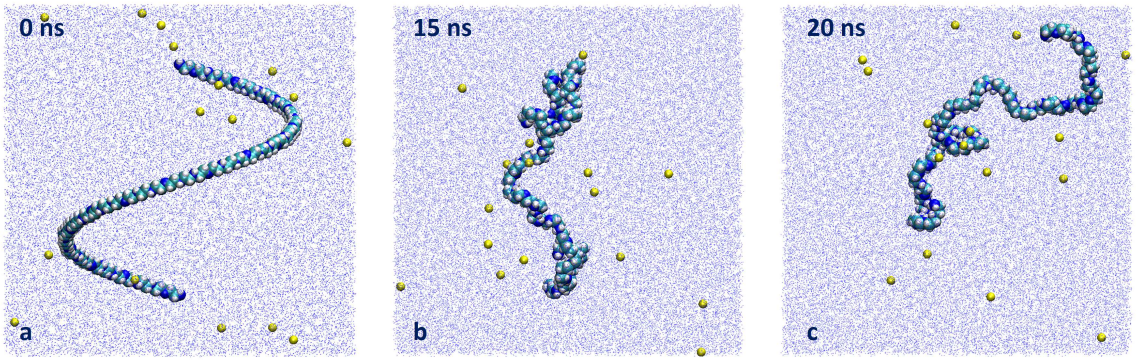

FIGURE 1. (a) Initial configuration with randomly placed water molecules and chloride ions around a helicoidal PEI 50-mer with 1/3 protonation fraction, (b) intermediate configuration and (c) final random-coil configuration of a typical trajectory).

For each PEI length and protonation fraction, we performed NPT runs extending over 20 ns, preceded by equilibration periods of 20 ps. Snapshots from a typical run for a 1/3-protonated 50-mer are depicted in Figure 1, showing the different conformational states of the polymer chain (initial helicoidal, intermediate, and final configuration). In order to reduce time correlations and improve statistics, the quantities of interest (gyration radius, end-to-end distance, radial distribution functions, and diffusion coefficients) were determined by averaging over 40 trajectories, each started from a different random initial configuration.

The extent of PEI chains is characterized in terms of gyration radius (R_g) and end-to-end distance (D_{ee}), calculated as the root mean square distance between the two terminal nitrogen atoms. Figure 2 comparatively shows the ensemble- and time-averaged values of R_g and D_{ee} as functions of the protonation fraction. While for the shortest polymer, the proles show quite reduced dependence on the chain protonation, the differences gradually increase for the longer PEI chains. The error bars can be seen to be reduced, and this is due to the extended cumulative time of the trajectory ensembles, amounting to 680 ns for each polymer configuration.

For a freely-jointed (ideal) chain, the D_{ee}/R_g ratio can be demonstrated to be equal to $\sqrt{6} \approx 2.45$. In excellent agreement, we find ratios for the unprotonated chains departing by less than 1% from the ideal value. While the simple freely-jointed model successfully applies to unprotonated chains, the D_{ee}/R_g ratios that we obtained for protonated

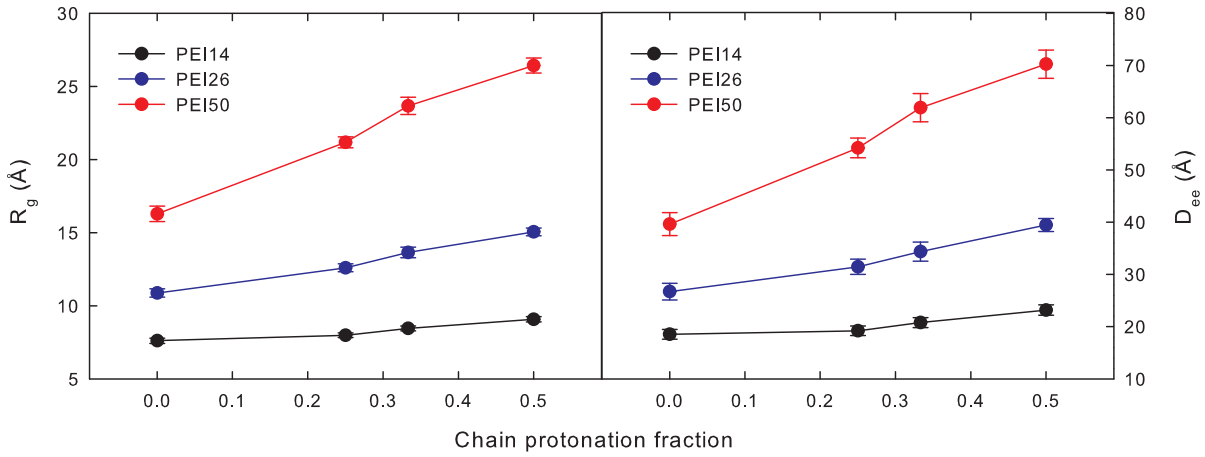

FIGURE 2. Variation of the gyration radius and end-to-end distance for uniformly protonated PEI 14, 26 and 50-mers with the protonation fraction.

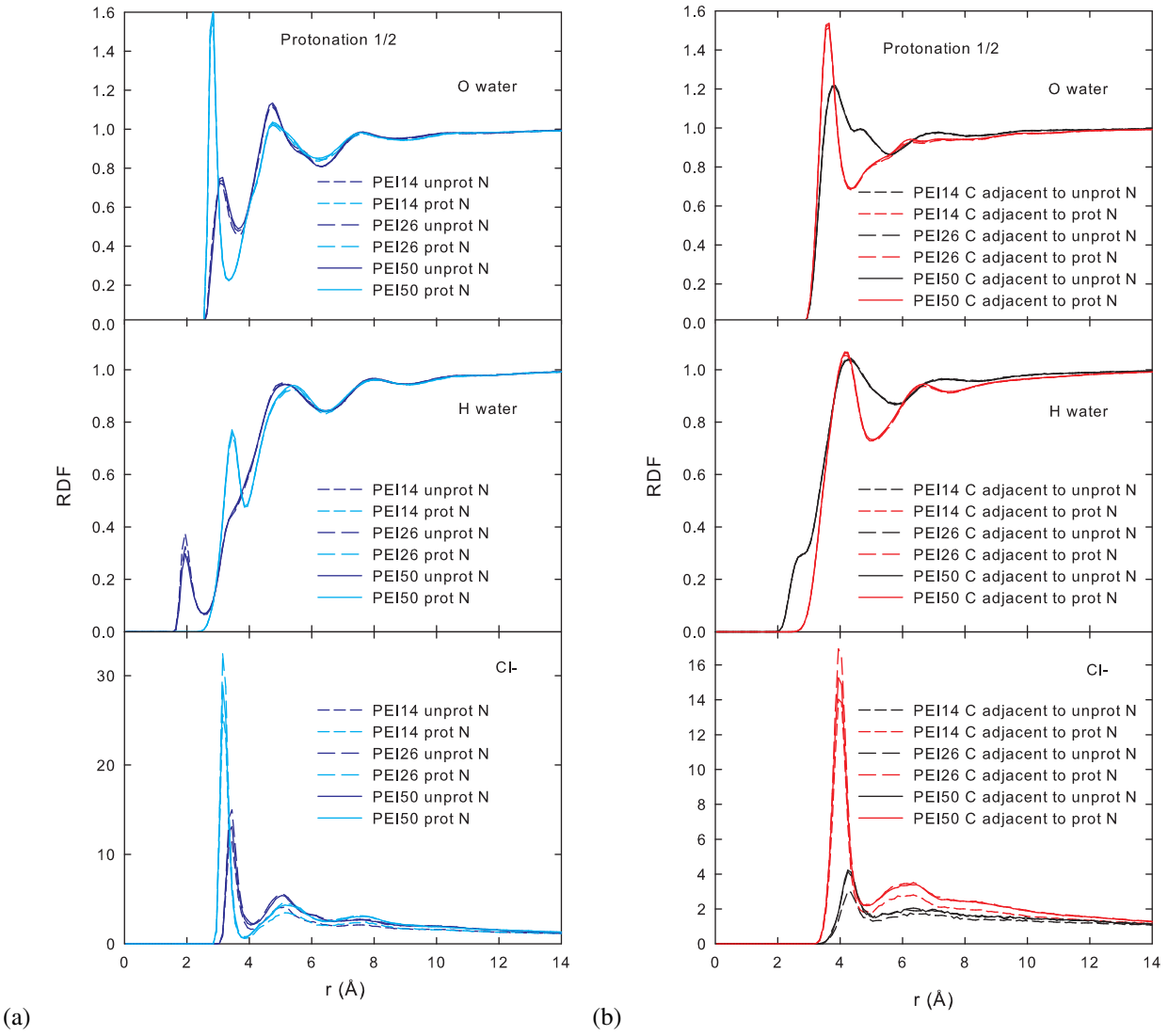

FIGURE 3. Radial distribution functions for the N atoms (left) and C atoms (right) of alternatively protonated PEI chains, respectively with the O (upper panel) and H (middle panel) atoms of water, and the Cl^- ions (lower panel).

chains increasingly deviate, reaching 2.65 for the alternatively protonated 50-mer. The supplementary electrostatic repulsion between the protonated units is obviously responsible for less compact configurations and, implicitly, for higher D_{ee}/R_g ratios.

To quantify the influence of the protonation fraction on the interaction of the PEI chains with the surrounding solvent and to describe the structural arrangement in the vicinity of the composing atomic species, we calculated the radial distribution functions (RDFs). The denser envelopes of water (hydration layers) prevent the polymer units that come in close proximity from forming hydrogen bonds.

The RDFs depicted in Figure 3a illustrate different affinities of the N species for the Cl^- ions and for the O and H atoms of the water molecules, respectively. Each plot features two prominent peaks, indicating two well-separated solvation shells around the N species. For all studied systems, the O atoms appear to be located on average closer to the protonated N than the H atoms and the Cl^- counterions. The two RDF patterns for unprotonated/protonated N become quite different beyond the first coordination shell. The first peak in the N-H profiles is smaller than in the N-O and N-Cl^- case. This suggests that hydrogen bonding is dominated by the N-O Coulomb interactions, which control

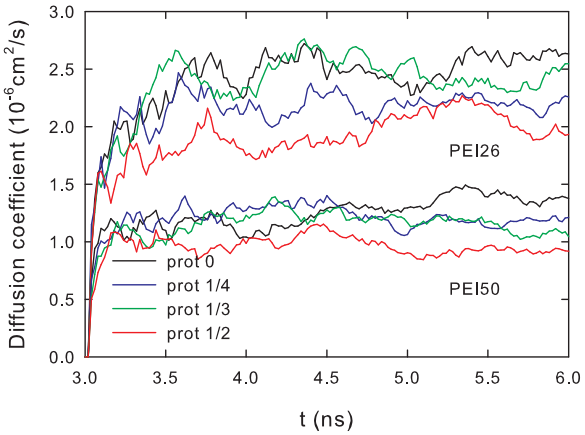

FIGURE 4. Diffusion coefficients for uniformly protonated 26 and 50-mers of PEI chains.

the solvation of the PEI chains.

The charge on the NH_2^+ group is higher than on the NH group, which leads to an increased density of negative Cl^- and O atoms about the protonated N species. Corroborating the N-O and N-H RDFs, from the closer positioning of the H-shell as compared to the O-shell, the water molecules appear to be predominantly oriented with the dipole moment *towards* the unprotonated N. By contrast, the dipole moment of the water molecules points on average *away* from the protonated N.

Figure 3b presents RDFs similar to those in Figure 3a for the considered chain sizes, however with the C atoms of the PEI chains as reference. From the relative positions of the O- and H-peaks, an orientation of the water dipole moment with respect to the C species similar to the adjacent N species can be inferred. Whereas the Cl^- RDFs for the C species adjacent to protonated N show a noticeable drop with increasing chain size, for C adjacent to unprotonated N a slight increase is apparent. This behavior is rather geometrical in nature, being linked to the the fact that for a given protonation fraction, while the number of neutralizing counterions is proportional to the chain length, the volume of the simulation box size grows at a higher rate, and, correspondingly, the ion concentration decreases faster than linearly.

A quantity illustrating the dynamic behavior of solvated polymers is the diffusion coefficient, and we estimated it based on Einstein's relation:

$$D = \lim_{t\to\infty} \frac{1}{6t} < [r(t) - r(0)] >^2 \tag{4}$$

As the main ingredient, the mean squared displacement measures the spread of the positions of the polymer's center of mass in time, by cumulating the squared differences between the instantaneous and initial positions.

Figure 4 shows the time dependence of the center of mass diffusion coefficient of the solvated PEI 26-mer and 50-mer for the various protonation fractions. The saturation levels clearly emphasize the significant drop of the diffusion coefficient both with the chain size and protonation fraction, and this is consistent with the increased average spatial extents described by the gyration radius and end-to-end distance. The significant effect of protonation on the PEI chain dynamics suggests an effective way of controlling the PEI mobility.

CONCLUSIONS

We report atomistic molecular dynamics simulations of structure and dynamics of solvated polyethylenimine (PEI). We considered polymer chain sizes and protonation fractions in the range of the experimentally available data.

The radius of gyration and end-to-end distance, R_g and D_{ee}, synthetically characterizing the average spatial extent of the polymer chains, increase with the chain size and protonation fraction. For unprotonated PEI chains, the D_{ee}/R_g ratio compares very well with the value for the freely-jointed chain model.

The radial distribution functions provide a detailed description of the Cl^- counterion distribution and water molecule orientation about the backbone atoms of the PEI chains. The protonated/unprotonated N species are surrounded by hydration shells with opposed average dipole moments. In spite of their very low concentrations, the neutralizing Cl^- ions form sharp peaks about the N and C backbone atoms.

The diffusion coefficient of the PEI chains strongly decreases with the chain size and protonation fraction, alternatively protonated 50-mers showing the smallest mobilities.

ACKNOWLEDGMENTS

This work was supported by a grant of the Romanian Ministry of Research and Innovation, CNCS-UEFISCDI, project number PN-III-P4-ID-PCE-2016-0474.

REFERENCES

1. F. D. Ledley, Human Gene Therapy **6**, 1129–1144 (1996).
2. W. M. Saltzman and D. Luo, Nature Biotechnology **18**, 33–37 (2000).
3. N. Nayerossadat, P. Ali, and T. Maedeh, Advanced Biomedical Research **1**, p. 27 (2012).
4. C. E. Thomas, A. Ehrhardt, and M. A. Kay, Nature Reviews Genetics **4**, 346–358 (2003).
5. M. A. Mintzer and E. E. Simanek, Chem. Rev. **109**, 259–302 (2009).
6. J. W. Wiseman, C. A. Goddard, D. McLelland, and W. H. Colledge, Gene Therapy **10**, 1654–1662 (2003).
7. O. Boussif, F. Lezoualc'h, M. A. Zanta, M. D. Mergny, B. D. D. Scherman, and J. P. Behr, Proc. Natl. Acad. Sci. U.S.A. **92**, 7297–7301 (1995).
8. W. T. Godbey and A. G. Mikos, J. Control. Release **72**, 115–125 (2001).
9. M. Morille, C. Passirani, A. Vonarbourg, A. Clavreul, and J. P. Benoit, Biomaterials **29**, 3477–3496 (2008).
10. R. V. Benjaminsen, M. A. Mattebjerg, J. R. Henriksen, S. M. Moghimi, and T. L. Andresen, Molecular Therapy **21**, 149–157 (2013).
11. J. D. Ziebarth and Y. Wang, Biomacromolecules **11**, 29–38 (2010).
12. C. Sun, T. Tang, H. Uludağ, and J. E. Cuervo, Biophysical J. **100**, 2754–2763 (2011).
13. Z. Wei and E. Luijten, J. Chem. Phys. **143**, p. 243146 (2015).
14. A. D. MacKerell, D. Bashford, M. Bellott, R. L. Dunbrack, J. D. Evanseck, M. J. Field, S. Fischer, J. Gao, H. Guo, S. Ha, D. Joseph-McCarthy, L. Kuchnir, K. Kuczera, F. T. Lau, C. Mattos, S. Michnick, T. Ngo, D. T. Nguyen, B. Prodhom, W. E. Reiher, B. Roux, M. Schlenkrich, J. C. Smith, R. Stote, J. Straub, M. Watanabe, J. Wiorkiewicz-Kuczera, D. Yin, and M. Karplus, J. Phys. Chem. B **102**, 3586–3616 (1998).
15. K. Vanommeslaeghe, E. Hatcher, C. Acharya, S. Kundu, S. Zhong, J. Shim, E. Darian, O. Guvench, P. Lopes, I. Vorobyov, and A. D. MacKerell, J. Comput. Chem. **31**, 671–690 (2010).
16. J. C. Phillips, R. Braun, W. Wang, J. Gumbart, E. Tajkhorshid, E. Villa, C. Chipot, R. D. Skeel, L. Kale, and K. Schulten, J. Comput. Chem. **26**, 1781–1802 (2005).
17. S. Miyamoto and P. A. Kollman, Journal of Computational Chemistry **13**, 952–962 (1992).
18. U. Essmann, L. Perera, M. L. Berkowitz, T. Darden, H. Lee, and L. G. Pedersen, J. Chem. Phys. **103**, 8577–8593 (1995).
19. W. Humphrey, A. Dalke, and K. Schulten, J. Molec. Graphics **14**, 33–38 (1996).
20. T. A. Beu and A. Farcaş, Journal of Computational Chemistry (2017), 10.1002/jcc.24890.
21. W. L. Jorgensen, J. Chandrasekhar, J. D. Madura, R. W. Impey, and M. L. Klein, J. Chem. Phys. **79**, 926–935 (1983).